

Mitigating Barren plateaus in quantum denoising diffusion probabilistic models

Haipeng Cao^{1*} Kaining Zhang^{2*} Dacheng Tao² Zhaofeng Su^{3,1†}

¹ School of Computer Science and Technology, University of Science and Technology of China

² College of Computing and Data Science, Nanyang Technological University

³ Research Institute for Quantum Technology, The Hong Kong Polytechnic University

Abstract

Quantum generative models leverage quantum superposition and entanglement to enhance learning efficiency for both classical and quantum data. The quantum denoising diffusion probabilistic model (QuDDPM), inspired by its classical counterpart, has been proposed as a promising framework for quantum generative learning. QuDDPM is capable of efficiently learning and generating quantum data, and it demonstrates excellent performance in learning correlated quantum noise models, quantum many-body phases, and the topological structure of quantum data. However, we show that barren plateaus emerge in QuDDPMs due to the use of 2-design states as the input for the denoising process, which severely undermines the performance of QuDDPM. Through theoretical analysis and experimental validation, we confirm the presence of barren plateaus in the original QuDDPM. To address this issue, we introduce an improved QuDDPM that utilizes a distribution maintaining a certain distance from the Haar distribution, ensuring better trainability. Experimental results demonstrate that our approach effectively mitigates the barren plateau problem and generates samples with higher quality, paving the way for scalable and efficient quantum generative learning.

1 Introduction

Classical generative models are utilized to learn and generate classical data, such as language and images. The Transformer [1] is one of the representative generative models. Due to its ability to effectively capture long-range dependencies in sequential information and allowing parallel model computation, it has gained widespread attention in the field of artificial intelligence, especially in natural language processing. The generative adversarial network (GAN) [2] introduces the idea of adversarial generation, offering a new approach for generative models. However, due to issues such as mode collapse in the model, effective training can be rather challenging [3]. Variational autoencoders (VAE) [4] can learn the latent distribution of data to achieve high-quality data generation. However, the variational lower bound of VAEs can lead to underfitting, and using a tighter bound doesn't guarantee better generation [5]. Subsequent denoising diffusion probabilistic models (DDPM) [6] have been proposed. These models decompose the data generation process into multiple simple denoising steps, enabling the generation of higher quality data while maintaining relatively stable training. However, due to the inclusion of numerous denoising steps, the data generation process is relatively slow, and these models typically have a large number of parameters and higher computational resource requirements.

*Equal Contribution.

†Corresponding author: Zhaofeng Su (zhaofsu@polyu.edu.hk).

In recent years, quantum machine learning has garnered considerable attention in both academic and business circles. Many significant concepts and interesting models in classical machine learning have been generalized to quantum scenario. Quantum Generative Learning Models (QGLMs) have recently gained significant attention due to their efficient processing of high-dimensional data and their powerful generative capabilities [7]. Several quantum generative models have been proposed, such as quantum generative adversarial networks (QuGAN) [8, 9], quantum variational autoencoder (QVAE) [10], and quantum circuit born machines (QCBM) [11, 12]. However, these models still have flaws. QuGANs still suffers from mode collapse, making the model hard to train [13]. QCBMs are sensitive to loss function selection. An improper loss function can lead to ineffective data distribution learning. Additionally, QCBMs have limited capability in handling continuous data and cannot achieve effective learning on such data [12].

Because of its stability, interpretability, flexibility, relatively simple training scheme, and capability to generate higher quality data, the DDPM model has gained widespread attention. Consequently, in the field of quantum machine learning, the quantum diffusion probabilistic model (QuDDPM), which can efficiently learn and generate quantum data, has been developed based on classical DDPM [14]. QuDDPM uses sufficient circuit layers to ensure expressiveness and introduces multiple intermediate training tasks to guarantee efficient training, achieving an efficiently trainable quantum data generation model. In addition, the QuDDPM demonstrates excellent performance in learning correlated quantum noise models, quantum many-body phases, and the topological structure of quantum data. In the classical world, QuDDPM may also have significant potential for classic generative tasks such as modeling classic data distributions and image generation. Therefore, QuDDPM has great potential in generative tasks.

However, we have identified a critical drawback in QuDDPM. Since its denoising process uses Haar-random states as inputs, it is highly likely to suffer from the barren plateau phenomenon. In this case, the training gradient of the model decreases exponentially with an increasing number of qubits, ultimately rendering the model untrainable. In this work, we delve into the intriguing yet challenging barren plateau phenomenon in QuDDPMs, aiming to pave the way for more effective quantum diffusion models. Our comprehensive simulations reveal a compelling phenomenon: as the quantum data dimension (i.e., qubit count) escalates, the gradients diminishes exponentially towards zero, strongly suggesting the presence of barren plateaus in QuDDPMs. To further substantiate this observation and investigate the underlying causes, we carried out a rigorous theoretical analysis of how the initial inputs to the denoising process affect the training gradient. The theoretical results align perfectly with our experimental findings.

Armed with our finding, we introduce an innovative method to mitigate the barren plateau issue. By strategically controlling the parameters of the forward diffusion process, we can steer the resulting distribution away from the problematic Haar distribution, which in turn serves as a more favorable foundation for training the backward process. At this point, the input to the denoising process can be a state that has a certain distance from the Haar-random distribution, thereby alleviating the barren plateau phenomenon. To elaborate on our proposed solution, we carry out a meticulous theoretical analysis of the improved QuDDPM. Our experimental simulations not only corroborate our theoretical analysis but also demonstrate that our approach effectively alleviates the barren plateau dilemma and significantly boosts the performance of the QuDDPM. This work holds great promise for advancing the field of quantum diffusion models and unlocking their full potential in various quantum - related applications.

Our pioneering contributions in this paper are:

- We are the first to reveal that QuDDPM suffers from the barren plateau problem. Through rigorous theoretical and experimental proof, we demonstrate the existence of barren plateaus and its underlying causes.
- We discuss how the barren plateaus in QuDDPM differ from those typically caused by circuit depth. Our analysis reveals that the barren plateaus in QuDDPM have a more severe impact on the model.
- We propose an innovative solution to effectively alleviate the barren plateau issue in QuDDPM. And we experimentally verify the effectiveness of the improved QuDDPM.

2 Preliminary

2.1 Notations and quantum computing knowledge

2.1.1 Notations

We denote by $\text{Tr}[\cdot]$ the trace of a matrix. The n -dimensional vector with each element being one is denoted as $\mathbf{1}_n$. The tensor product operation is denoted as \otimes . The conjugate transpose of a matrix U is denoted as U^\dagger . We denote by $\partial_k \mathcal{L}(\boldsymbol{\theta})$ the partial derivative of the function $\mathcal{L}(\boldsymbol{\theta})$ with respect to θ_k , where $\boldsymbol{\theta}$ is a vector. The mean and the variance of a random variable are denoted by $\langle \cdot \rangle$ and $\text{Var}(\cdot)$, respectively. The complex conjugate of a complex number x is denoted as \bar{x} . The Kronecker symbol is denoted by δ_{ij} . We denote by $\mathcal{U}(N)$ the group of $N \times N$ unitary matrices.

2.1.2 Quantum computing

Quantum state. Any quantum system is associated with a Hilbert space known as its state space. The pure state of the system can be completely described by a unit vector in the state space, represented by the Dirac notation $|\cdot\rangle$. Quantum bit, abbreviated as *qubit*, is the unit of quantum computing, which can be in the state $|0\rangle \equiv (1, 0)^T$ or $|1\rangle \equiv (0, 1)^T$. A general qubit can be in the superposition state $|\psi\rangle = \alpha|0\rangle + \beta|1\rangle$, where $\alpha, \beta \in \mathbb{C}$ and $|\alpha|^2 + |\beta|^2 = 1$. A pure N -qubit state $|\psi\rangle = \sum_{k=0}^{2^N-1} \alpha_k |k\rangle$ lies in the tensor product of N single-qubit spaces. Any state can be written as a density operator $\rho = |\psi\rangle\langle\psi|$, where $\langle\psi| = |\psi\rangle^\dagger$.

Quantum gates. Similar with the logical circuits in classical computing, quantum gates act on qubits in quantum computing. A quantum gate can be regarded as a unitary operator on the state space. Commonly used single-qubit unitary operators include $R_X(\theta) = e^{-i\theta X/2}$, $R_Y(\theta) = e^{-i\theta Y/2}$, and $R_Z(\theta) = e^{-i\theta Z/2}$, where

$$X = \begin{pmatrix} 0 & 1 \\ 1 & 0 \end{pmatrix}, Y = \begin{pmatrix} 0 & -i \\ i & 0 \end{pmatrix}, Z = \begin{pmatrix} 1 & 0 \\ 0 & -1 \end{pmatrix}. \quad (1)$$

X , Y and Z are called Pauli matrices, $\{I, X, Y, Z\}$ can be represented by $\{\sigma_0, \sigma_1, \sigma_2, \sigma_3\}$. A commonly employed two-qubit operator is the controlled Z gate:

$$CZ = \begin{pmatrix} 1 & 0 & 0 & 0 \\ 0 & 1 & 0 & 0 \\ 0 & 0 & 1 & 0 \\ 0 & 0 & 0 & -1 \end{pmatrix}. \quad (2)$$

and $R_{ZZ_{k_1, k_2}}(\theta)$:

$$R_{ZZ_{k_1, k_2}}(\theta) = \begin{pmatrix} e^{-i\theta/2} \mathbf{I}_2 & \mathbf{0}_2 \\ \mathbf{0}_2 & e^{i\theta/2} \mathbf{I}_2 \end{pmatrix}, \quad (3)$$

where

$$\mathbf{I}_2 = \begin{pmatrix} 1 & 0 \\ 0 & 1 \end{pmatrix}, \mathbf{0}_2 = \begin{pmatrix} 0 & 0 \\ 0 & 0 \end{pmatrix}. \quad (4)$$

Quantum measurement. In quantum computation, projective measurements are commonly used for observing computing results. A projective measurement is described by an observable M , which is a Hermitian operator on the state space with a spectral decomposition $M = \sum_m m P_m$. Note that P_m is the projector onto the eigenspace of M with eigenvalue m and correspond to any possible measurement outcomes. Upon measuring the state $|\psi\rangle$, the probability of observing m is given by $p(m) = \langle\psi|P_m|\psi\rangle$. On observing m , the state immediately after the measurement is $\frac{P_m|\psi\rangle}{\sqrt{p(m)}}$.

2.2 Barren plateaus in quantum machine learning

Barren plateaus refer to the common phenomena in quantum machine learning that training gradients exponentially approach zero as the number of qubits increases. This often results in a decline in model trainability and can even render models untrainable. The barren plateaus may originate from a diverse reasons such as circuit expressiveness, input data entanglement, or noise [15, 16, 17, 18].

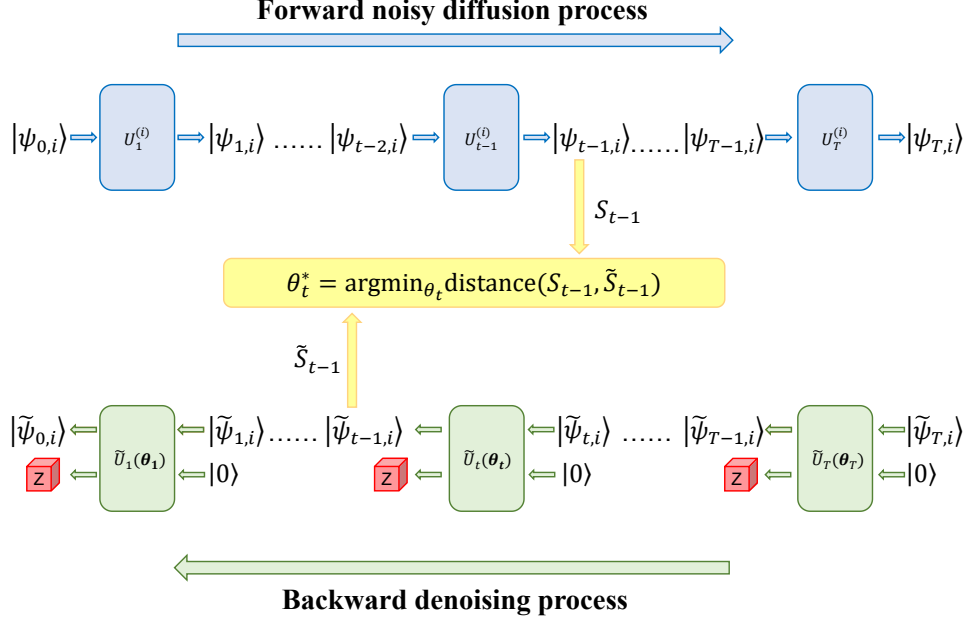


Figure 1: Structure of QuDDPM. The top part of the figure shows the forward noisy diffusion process and the bottom part shows the backward denoising process.

The initial study found that the barren plateau occurs when variational circuits form unitary 2-design distributions [15]. After that, researchers have found that highly entangled random states, arising from unitary transformations being randomly sampled with independent rotation angles, can lead to barren plateaus [16, 17]. Furthermore, studies show that noisy quantum channels can also induce the barren plateaus during training of variational quantum algorithms [18].

Several works have been focused on solving or mitigating the barren plateau problem. Specifically, efforts have shown that limiting the effective depth of circuits through initialization could avoid the barren plateaus [19, 20]. Additionally, barren plateaus can be mitigated by reducing ansatz expressibility, such as correlating parameters or restricting rotation angles [21].

2.3 Overview of QuDDPM

The recently proposed QuDDPM is the state-of-the-art quantum generation model, which was inspired by classical DDPMs. QuDDPM aims to generate new samples by learning from an ensemble of samples in the target distribution. This is accomplished by feeding samples from the target distribution into the forward diffusion process to add noise until they become Haar random states, and training the backward denoising process to invert the forward diffusion. Once training is complete, new samples can be generated by implementing the trained backward denoising process.

Structure of QuDDPM. As shown in Fig. 1, QuDDPM is composed of a forward noisy diffusion process via quantum scrambling and a backward denoising process via quantum measurement. Both processes contain T intermediate unitary gates to accomplish their tasks.

Forward diffusion process. In the forward diffusion process, the role of quantum scrambling circuit (QSC) $U_t^{(i)}$ is to add noise to the input state $|\psi_{t-1,i}\rangle$, making it deviate from the original distribution \mathcal{D}_{t-1} . Therefore, when all states $|\psi_{t-1,i}\rangle$ in ensemble \mathcal{S}_{t-1} pass through $U_t^{(i)}$, ensemble \mathcal{S}_{t-1} is transformed into a new ensemble \mathcal{S}_t corresponding to a noise-added distribution \mathcal{D}_t . After T applications of $U_t^{(i)}$, the final ensemble \mathcal{S}_T corresponds to the Haar distribution.

Backward denoising process. In the backward process, QuDDPM takes the ensemble $\tilde{\mathcal{S}}_T = \{|\tilde{\psi}_{T,i}\rangle\}$, sampled from the Haar distribution, as the input of the first training cycle. For each state $|\tilde{\psi}_{T,i}\rangle$, after undergoing the processing of $T - t$ variational parametrized quantum circuits (PQC)

$\tilde{U}_k(\theta_k)$, which act on the system plus n_a ancilla qubits in $|0\rangle$ and perform a projective measurement in computational bases on the ancilla at the end of the circuit, the ensemble $\tilde{\mathcal{S}}_t = \{|\tilde{\psi}_{t,i}\rangle\}$ is generated, which is similar to \mathcal{S}_t . Thus, for each ensemble \mathcal{S}_t from \mathcal{S}_{T-1} to \mathcal{S}_0 , the denoising process trains the corresponding $\tilde{U}_t(\theta_t)$ sequentially to make the generated ensemble $\tilde{\mathcal{S}}_t$ as similar as possible to \mathcal{S}_t , ultimately producing an ensemble $\tilde{\mathcal{S}}_0$ that conforms to the target distribution \mathcal{D}_0 . The general circuit structure of the $\tilde{U}_t(\theta_t)$ is given as follows:

$$\tilde{U}_t(\theta_t) = \prod_{l=1}^L W_l V_l(\theta_{t,l}), \quad (5)$$

where W_l is a generic unitary operator that does not depend on any angle θ , $V(\theta_{t,l}) = \bigotimes_{\lambda=0}^{n-1} R_{\sigma^{(i)}}(\theta_{t,l,\lambda\tau+i})$, $\sigma^{(i)} \in \{\sigma_1, \sigma_2, \sigma_3\}$, n is the total number of qubits.

Generation stages. Input a Haar random state into the trained reverse denoising process and execute it, the final state generated is a sample that match the target distribution \mathcal{D}_0 .

Loss function. In training, measuring the distance between generated and real data is essential. To achieve this, Maximum Mean Discrepancy (MMD) is introduced as the loss function. The MMD formula is as follows:

$$\mathcal{D}_{\text{MMD}}(\mathcal{S}_1, \mathcal{S}_2) = \bar{F}(\mathcal{S}_1, \mathcal{S}_1) + \bar{F}(\mathcal{S}_2, \mathcal{S}_2) - \bar{F}(\mathcal{S}_1, \mathcal{S}_2), \quad (6)$$

where $\bar{F}(\mathcal{S}_1, \mathcal{S}_2) = \mathbb{E}_{|\phi\rangle \in \mathcal{S}_1, |\psi\rangle \in \mathcal{S}_2} [|\langle \phi | \psi \rangle|^2]$, both \mathcal{S}_1 and \mathcal{S}_2 is quantum state ensembles. Notably, since the generated data $\tilde{\mathcal{S}}_{t-1}$ is smaller than the real data \mathcal{S}_{t-1} , the distance calculated between them is typically the distance between $\tilde{\mathcal{S}}_{t-1}$ and a subset \mathcal{S}'_{t-1} of \mathcal{S}_{t-1} , which has the same size as $\tilde{\mathcal{S}}_{t-1}$. That is, the loss function is given by:

$$\mathcal{L}_t(\theta_t) = \mathcal{D}_{\text{MMD}}(\tilde{\mathcal{S}}_{t-1}, \mathcal{S}'_{t-1}) = \mathcal{D}_{\text{MMD}}(\tilde{U}_t(\theta_t)\tilde{\mathcal{S}}_t, \mathcal{S}'_{t-1}). \quad (7)$$

3 Theoretical results

3.1 Theoretical analysis of barren plateau

In this subsection, we present an analysis of the barren plateau caused by the input of the PQCs. Recall that barren plateaus represent gradients exponentially approaching zero, so our analysis will focus on gradients of the loss function in Eq. 7.

The loss function Eq. 7 can be viewed as a function of the unitary operator $\tilde{U}_t(\theta_t)$, so we need to first compute the derivative of $\tilde{U}_t(\theta_t)$ with respect to θ_t before calculating the gradients of the loss. Therefore, we calculate the gradient of the unitary operator $\tilde{U}_t(\theta_t)$ with respect to the parameter $\theta_{t,l,k}$ as follows:

$$\partial_{l,k} \tilde{U}_t(\theta_t) = -\frac{i}{2} \tilde{U}_{t,L:l} K \tilde{U}_{t,l-1:1}, \quad (8)$$

where $\alpha = k \bmod \tau$, n is the total number of qubits, $K = (\bigotimes_{\lambda=0}^{n-1} \prod_{i=\alpha+1}^{\tau-1} R_{\sigma^{(i)}}(\theta_{t,l,\lambda\tau+i}))^\dagger [(I^{0:[k/\tau]}]$

$\otimes \sigma^{(\alpha)} \otimes I^{[k/\tau+1]:n}) (\bigotimes_{\lambda=0}^{n-1} \prod_{i=\alpha+1}^{\tau-1} R_{\sigma^{(i)}}(\theta_{t,l,\lambda\tau+i}))$, $I^{i:j}$ denotes that the operator I acts on the qubits

in the range $[i, j]$. Obviously, K is a Hermitian operator. Furthermore, for $\tilde{U}_t(\theta_t)$ with multiple layers, we define $\tilde{U}_{t,l_1:l_2} = \prod_{l=l_2}^{l_1} W_l V_l(\theta_{t,l})$. The proof of Eq. 8 is provided in Appendix.

Therefore, we can obtain the gradient of the loss function Eq. 7 with respect to the parameter $\theta_{t,l,k}$ as follows:

$$\partial_{l,k} \mathcal{L}_t = \frac{i}{|\mathcal{S}|^2} \sum_{i,j} \text{Tr}(|\psi_{t-1,j}\rangle \langle \psi_{t-1,j}| \cdot \tilde{U}'_{t,L:l} [K, \tilde{U}'_{t,l-1:1} |\tilde{\psi}_{t,i}\rangle \langle \tilde{\psi}_{t,i}| \tilde{U}_{t,l-1:1}^\dagger] \tilde{U}_{t,L:l}^\dagger), \quad (9)$$

where $|\mathcal{S}| = |\mathcal{S}_{t-1}| = |\tilde{\mathcal{S}}_{t-1}|$, $|\psi_{t-1,j}\rangle \in \mathcal{S}_{t-1}$, $|\tilde{\psi}_{t,i}\rangle \in \tilde{\mathcal{S}}_t$, \tilde{U}'_t represents the part of \tilde{U}_t applied to the data qubits. The proof is provided in Appendix.

To elucidate the exponential decay of the loss function gradient with the increasing number of qubits, we first investigate its underlying cause. We observe that the initial input to the denoising process comprises Haar random states. This input leads to the observed gradient decay, aligning with the barren plateau phenomenon. Notably, this case differs from conventional barren plateau scenarios, which are typically associated with excessive circuit depth. Accordingly, we conduct a focused theoretical analysis of this distinct mechanism.

Moreover, we find that when the initial input to the denoising process is Haar random states and induces the barren plateau phenomenon, the states generated in the first training cycle will be approximate Haar random states. This still may trigger the barren plateau phenomenon. It means that it can trigger a chain reaction of barren plateaus when the backward denoising process takes Haar random states as inputs. This can render the entire training process untrainable, causing far more severe harm than the general barren plateau caused by circuit depth.

To demonstrate the hypotheses, we redefine the loss function for the scenario where the input to the PQC is Haar random states, as follows:

$$\partial_{l,k}\mathcal{L}_H = \frac{i}{|\mathcal{S}|^2} \sum_{i,j} \text{Tr}(|\psi_j\rangle\langle\psi_j| \cdot \tilde{U}'_{L:l}[K, \tilde{U}'_{l-1:1} \cdot U_{H_i}|0\rangle\langle 0|U_{H_i}^\dagger \cdot \tilde{U}'_{l-1:1}]\tilde{U}'_{L:l}), \quad (10)$$

where $U_{H_i} \in \mathcal{U}_H(N)$ obeying Haar measure, $N = 2^{n_{data}}$, n_{data} is the number of data qubits; the loss function when the input to the PQC is approximate Haar random states as follows:

$$\partial_{l,k}\mathcal{L}_A = \frac{i}{|\mathcal{S}|^2} \sum_{i,j} \text{Tr}(|\psi_j\rangle\langle\psi_j| \cdot \tilde{U}'_{L:l}[K, \tilde{U}'_{l-1:1} \cdot U_{A_i}|0\rangle\langle 0|U_{A_i}^\dagger \cdot \tilde{U}'_{l-1:1}]\tilde{U}'_{L:l}), \quad (11)$$

where $U_{A_i} \in \mathcal{U}_A(N)$ obeying approximate Haar measure.

Theorem 1. For Eq. 22 and Eq. 42, if $U_{H_i} \in \mathcal{U}_H(N)$ obeying Haar measure, $U_{A_i} \in \mathcal{U}_A(N)$ obeying approximate Haar measure, then:

$$\langle \partial_{l,k}\mathcal{L}_H \rangle = 0, \quad |\text{Var}(\partial_{l,k}\mathcal{L}_H)| \leq \frac{8}{|\mathcal{S}|^4 \cdot (2^{2n_{data}} - 1)}, \quad (12)$$

$$\langle \partial_{l,k}\mathcal{L}_A \rangle = \varepsilon, \quad |\text{Var}(\partial_{l,k}\mathcal{L}_A)| \leq \frac{8}{|\mathcal{S}|^4 \cdot (2^{2n_{data}} - 1)} + 4\zeta. \quad (13)$$

where n_{data} is the number of data qubits, ε, ζ denote the deviations of approximate Haar random states from exact Haar random states at different angles. For detailed definitions, see Appendix.

As shown in Theorem 1, it is clear that as the number of qubits increases, the variance of the gradient is upper bounded by the term that converges exponentially to zero as the number of qubits increases. Therefore, when the number of qubits increases, the gradient will converge exponentially to mean 0. This indicates that when the number of qubits is large, QuDDPM indeed suffers from the barren plateau phenomenon, which arises due to the use of Haar random states as inputs to the PQC. Therefore earlier PQCs aren't trained properly, later PQCs will receive approximately Haar random states as inputs. Consequently, the entire training process is hindered by the barren plateau phenomenon, making the model untrainable. In this scenario, the impact of the barren plateau phenomenon is far more severe than that caused by circuit depth.

3.2 Improved QuDDPM and Its Effectiveness Analysis

We have shown that QuDDPM suffers from barren plateaus caused by input states that match the Haar distribution. To address this, we improve QuDDPM by modifying its input for the denoising process. Specifically, we ensure that the states produced by the forward diffusion process maintain a certain distance from the Haar distribution. Additionally, we take the ensemble surrounding the $|0\rangle^{\otimes n_{data}}$ as the input for the forward process, and the resulting final state ensemble is used as the initial input for backward denoising process. We also provide a theoretical analysis of the effectiveness of the improved QuDDPM.

We provide the gradient analysis for the denoising training in QuDDPM in Theorem 2 with the proof in Appendix. Specifically, for parameters constrained around 0 with scales $s_l = \mathcal{O}(1/L)$, where L is the number of parameters in the denoising circuit, the expectation of the squared gradient could be

lower bounded by its value and the squared Hessian elements at $\theta = \mathbf{0}$ time additional terms that vanish at most polynomially. Intuitively, these terms could have large values for circuits consisting of layered W_l and local parameterized gates G_l , when both the initial state $|\tilde{\psi}\rangle$ and the target state $|\psi\rangle$ have large bias on local terms in their Pauli decompositions [22].

Theorem 2. Consider the function $f(\theta) = \text{Tr}[I \otimes |\psi\rangle\langle\psi| V(\theta) |0\rangle\langle 0| \otimes |\tilde{\psi}\rangle\langle\tilde{\psi}| V^\dagger(\theta)]$, where the VQC $V(\theta) = \prod_{l=L}^1 (W_l G_l(\theta_l)) = \prod_{l=L}^1 (W_l \exp[-i\theta_l H_l/2])$ consists of L parameterized gates G_l and fixed gates W_l . Suppose each Hamiltonian H_l is unitary and the corresponding parameter θ_l is sampled uniformly from $[-s_l, s_l]$. Then the squared gradient of f is bounded as follows:

$$\mathbb{E}_{\theta} \left(\frac{\partial f}{\partial \theta_k} \right)^2 \geq \left(\frac{\partial f}{\partial \theta_k}(\mathbf{0}) \right)^2 \prod_{l=1}^L \left(\frac{1}{2} + \frac{\sin 2s_l}{4s_l} \right) + H_{kk}(\mathbf{0})^2 \left(\frac{1}{2} - \frac{\sin 2s_k}{4s_k} \right) \prod_{l=1, l \neq k}^L \left(\frac{1}{2} + \frac{\sin 2s_l}{4s_l} \right), \quad (14)$$

where $H_{kk}(\mathbf{0}) = \frac{1}{2} \text{Tr} \left[W_{k-1:1} \rho W_{k-1:1}^\dagger [H_k, W_{L:k}^\dagger O W_{L:k} H_k] \right]$ is the (k, k) -th element of the Hessian of the function f at $\theta = \mathbf{0}$, $O := I \otimes |\psi\rangle\langle\psi|$, and $\rho := |0\rangle\langle 0| \otimes |\tilde{\psi}\rangle\langle\tilde{\psi}|$.

4 Experimental results

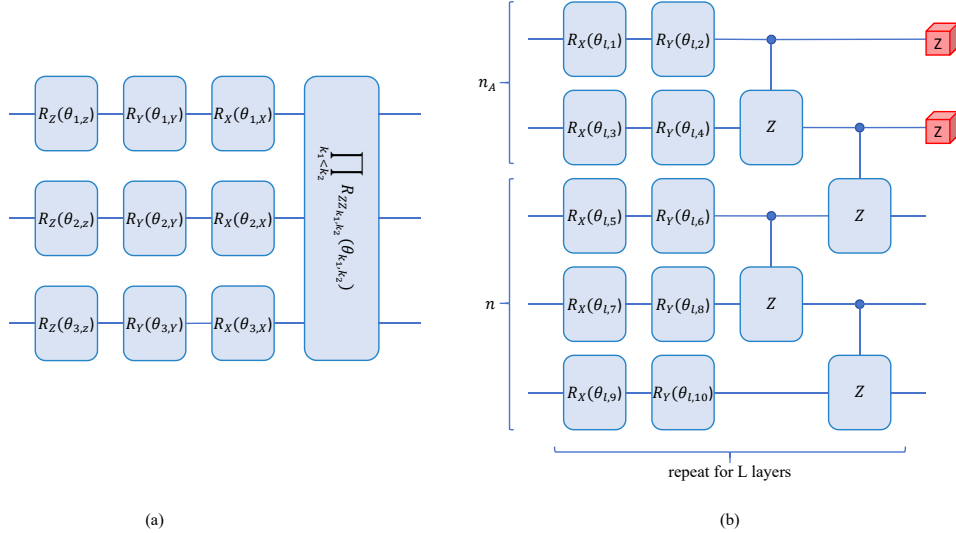


Figure 2: Quantum circuit architectures. (a) is the circuit of one step of the forward diffusion process on a system of $n = 3$ qubits. (b) is one-layer architecture of L -layer of $\tilde{U}_t(\theta_t)$ on a system of $n = 3$ data and $n_A = 2$ ancilla qubits.

To better illustrate the existence of barren plateaus in QuDDPM, we conducted corresponding experiments. In the experiment, we use the extended GHZ states $|\psi\rangle = \cos(\theta)|0\rangle^{\otimes n_{data}} + \sin(\theta)|1\rangle^{\otimes n_{data}}$ as the target data distribution, where $\theta \in [0, 2\pi]$. The diffusion circuit U_t^i and one-layer of denoising circuit $\tilde{U}_t(\theta_t)$ are shown in Fig. 2 (a) and (b), respectively. The detailed setup of the experiment is shown in Table 1. We will provide additional information about the experiments in Appendix.

In Fig. 3, we present the changes in the loss function of the original QuDDPM over the first six training cycles for different qubits. In Fig. 8, we present the changes in the gradient for the original QuDDPM and the improved QuDDPM over the first six training cycles as the number of qubits increases. We found that the decline trend of the loss function of the original QuDDPM rapidly decreased as the number of qubits increased, and its gradient also decreased exponentially, making it difficult to train the original QuDDPM. Correspondingly, the improved QuDDPM still maintains excellent trainability. This clearly indicates that original QuDDPM will suffer from the barren plateau phenomenon, rendering the model untrainable. In the appendix, we provide detailed variations of the gradients for different numbers of qubits over the first six training cycles.

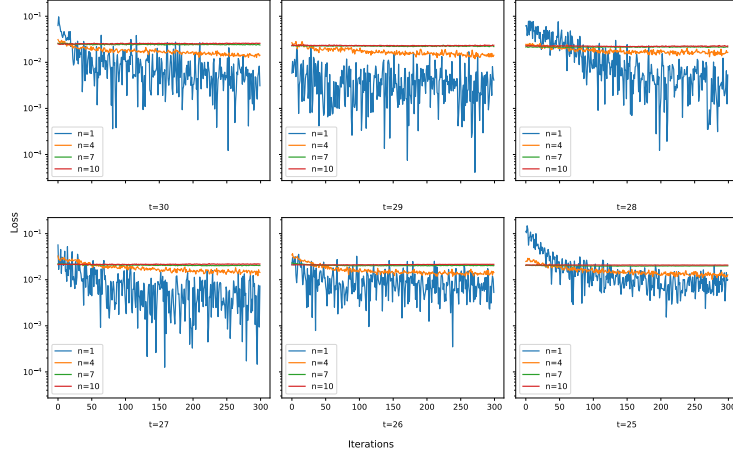


Figure 3: The evolution of the loss function of the original QuDDPM during the first six training cycles of the backward denoising process for different numbers of qubits.

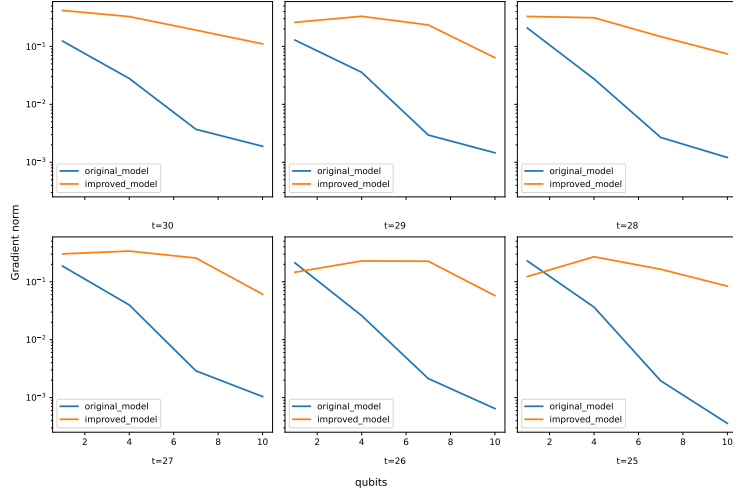


Figure 4: During the first six training cycles, the changes in the average training gradients of the improved and original QuDDPM systems as the number of qubits increased.

To demonstrate that our improved QuDDPM effectively mitigates the barren plateau problem, we compared the KL evolution of the improved QuDDPM and the original QuDDPM for 10 qubits. As shown in Fig. 5, the improved QuDDPM becomes trainable, and the quality of the generated samples is better than that of the original QuDDPM. To further illustrate that the improved QuDDPM effectively alleviates the barren plateau phenomenon, we present in the appendix a comparison of the gradient changes of the improved QuDDPM and the original QuDDPM during the first six training epochs in the noise reduction process for a 10-qubits system.

5 Limitations

As can be seen Fig. 5, even though the improved QuDDPM enhances the training effect compared to the original QuDDPM, the final sample quality still falls short of the ideal state. This reflects the issue of insufficient model expressiveness. This problem might be improved by increasing the number of training cycles. However, this often leads to a significant increase in the resources required for model

Table 1: Experimental Settings

Name	Description	Value
n_{data}	number of the data qubits	1/4/7/10
n_a	number of the ancilla qubits	3
T	number of the training cycles	30
epochs	number of iterations per training cycle	300
L	number of circuit layers of PQCs	5
lr	learning rate	0.005
optimizer	optimizer	Adam

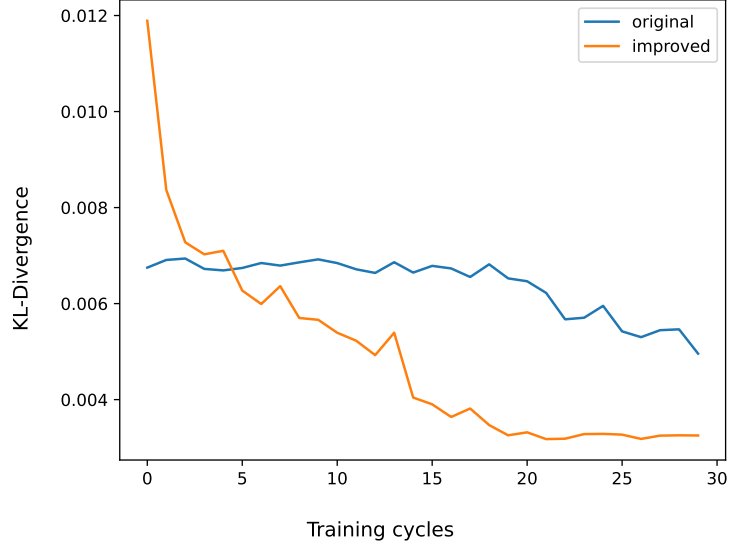


Figure 5: The KL divergence between the sample data generated at each denoising step by the improved QuDDPM and the original QuDDPM and the target data. This quantum system contains 10 qubits, that is, $n_{data} = 10$

training and a substantial extension of the training time. Therefore, a method is needed to enhance the model’s expressiveness without significantly increasing the resources required for model training.

6 Conclusions

In this work, we have demonstrated the barren plateau phenomenon in QuDDPM by proving that the mean of the training gradients is zero and that the variance decreases exponentially as the number of qubits increases. We have further corroborated this conclusion with corresponding experiments. Moreover, to address this issue, we propose a solution that involves restricting the parameters of the forward diffusion circuit so that the final distribution maintains a certain distance from the Haar distribution. For this method, we take the ensemble surrounding the $|0\rangle^{\otimes n_{data}}$ as the input for the forward process, and the resulting final state ensemble is used as the initial input of backward denoising process. We also provide theoretical analysis and experimental verification of the improved QuDDPM, concluding that the improved QuDDPM avoids barren plateaus to some extent. Future research will explore its approximation and expressive power for specific quantum state distributions, particularly physical quantum states that are classically hard to simulate and exhibit large local terms in their Pauli decomposition.

References

- [1] Ashish Vaswani, Noam Shazeer, Niki Parmar, Jakob Uszkoreit, Llion Jones, Aidan N Gomez, Lukasz Kaiser, and Illia Polosukhin. Attention is all you need. *Advances in Neural Information Processing Systems*, 30, 2017.
- [2] Ian Goodfellow, Jean Pouget-Abadie, Mehdi Mirza, Bing Xu, David Warde-Farley, Sherjil Ozair, Aaron Courville, and Yoshua Bengio. Generative adversarial networks. *Communications of the ACM*, 63(11):139–144, October 2020.
- [3] Kaifeng Zhang. On mode collapse in generative adversarial networks. In *International conference on artificial neural networks*, pages 563–574. Springer, 2021.
- [4] Yankun Chen, Jingxuan Liu, Lingyun Peng, Yiqi Wu, Yige Xu, and Zhanhao Zhang. Auto-encoding variational bayes. *Cambridge Explorations in Arts and Sciences*, 2(1), 2024.
- [5] Yuri Burda, Roger Grosse, and Ruslan Salakhutdinov. Importance weighted autoencoders. *arXiv preprint arXiv:1509.00519*, September 2015.
- [6] Jonathan Ho, Ajay Jain, and Pieter Abbeel. Denoising diffusion probabilistic models. *Advances in Neural Information Processing Systems*, 33:6840–6851, 2020.
- [7] Jinkai Tian, Xiaoyu Sun, Yuxuan Du, Shanshan Zhao, Qing Liu, Kaining Zhang, Wei Yi, Wanrong Huang, Chaoyue Wang, Xingyao Wu, Min-Hsiu Hsieh, Tongliang Liu, Wenjing Yang, and Dacheng Tao. Recent advances for quantum neural networks in generative learning. *IEEE Transactions on Pattern Analysis and Machine Intelligence*, 45(10):12321–12340, May 2023.
- [8] Pierre-Luc Dallaire-Demers and Nathan Killoran. Quantum generative adversarial networks. *Physical Review A*, 98(1):012324, July 2018.
- [9] Xun Gao, Z.-Y. Zhang, and L.-M. Duan. A quantum machine learning algorithm based on generative models. *Science Advances*, 4(12):eaat9004, December 2018.
- [10] Amir Khoshaman, Walter Vinci, Brandon Denis, Evgeny Andriyash, Hossein Sadeghi, and Mohammad H Amin. Quantum variational autoencoder. *Quantum Science and Technology*, 4(1):014001, September 2018.
- [11] Marcello Benedetti, Delfina Garcia-Pintos, Oscar Perdomo, Vicente Leyton-Ortega, Yunseong Nam, and Alejandro Perdomo-Ortiz. A generative modeling approach for benchmarking and training shallow quantum circuits. *npj Quantum Information*, 5(1):45, May 2019.
- [12] Jin-Guo Liu and Lei Wang. Differentiable learning of quantum circuit born machines. *Physical Review A*, 98(6):062324, December 2018.
- [13] Murphy Yuezhen Niu, Alexander Zlokap, Michael Broughton, Sergio Boixo, Masoud Mohseni, Vadim Smelyanskiy, and Hartmut Neven. Entangling quantum generative adversarial networks. *Physical Review Letters*, 128(22):220505, June 2022.
- [14] Bingzhi Zhang, Peng Xu, Xiaohui Chen, and Quntao Zhuang. Generative quantum machine learning via denoising diffusion probabilistic models. *Physical Review Letters*, 132(10):100602, March 2024.
- [15] Jarrod R McClean, Sergio Boixo, Vadim N Smelyanskiy, Ryan Babbush, and Hartmut Neven. Barren plateaus in quantum neural network training landscapes. *Nature Communications*, 9(1):4812, November 2018.
- [16] Carlos Ortiz Marrero, Mária Kieferová, and Nathan Wiebe. Entanglement-induced barren plateaus. *PRX Quantum*, 2(4):040316, October 2021.
- [17] Taylor L Patti, Khadijeh Najafi, Xun Gao, and Susanne F Yelin. Entanglement devised barren plateau mitigation. *Physical Review Research*, 3(3):033090, July 2021.
- [18] Samson Wang, Enrico Fontana, Marco Cerezo, Kunal Sharma, Akira Sone, Lukasz Cincio, and Patrick J Coles. Noise-induced barren plateaus in variational quantum algorithms. *Nature Communications*, 12(1):6961, November 2021.

- [19] Edward Grant, Leonard Wossnig, Mateusz Ostaszewski, and Marcello Benedetti. An initialization strategy for addressing barren plateaus in parametrized quantum circuits. *Quantum*, 3:214, December 2019.
- [20] Kaining Zhang, Liu Liu, Min-Hsiu Hsieh, and Dacheng Tao. Escaping from the barren plateau via gaussian initializations in deep variational quantum circuits. *Advances in Neural Information Processing Systems*, 35:18612–18627, 2022.
- [21] Zoë Holmes, Kunal Sharma, Marco Cerezo, and Patrick J Coles. Connecting ansatz expressibility to gradient magnitudes and barren plateaus. *PRX Quantum*, 3(1):010313, January 2022.
- [22] Kaining Zhang, Junyu Liu, Liu Liu, Liang Jiang, Min-Hsiu Hsieh, and Dacheng Tao. The curse of random quantum data. *arXiv preprint arXiv:2408.09937*, August 2024.
- [23] Zbigniew Puchała and Jarosław Adam Miszczyk. Symbolic integration with respect to the haar measure on the unitary group. *arXiv preprint arXiv:1109.4244*, September 2011.
- [24] Ville Bergholm, Josh Izaac, Maria Schuld, Christian Gogolin, Shah Nawaz Ahmed, Vishnu Ajith, M. Sohaib Alam, Guillermo Alonso-Linaje, B. AkashNarayanan, Ali Asadi, et al. PennyLane: Automatic differentiation of hybrid quantum-classical computations. *arXiv preprint arXiv:1811.04968*, July 2022.
- [25] Pauli Virtanen, Ralf Gommers, Travis E Oliphant, Matt Haberland, Tyler Reddy, David Cournapeau, Evgeni Burovski, Pearu Peterson, Warren Weckesser, Jonathan Bright, et al. Scipy 1.0: fundamental algorithms for scientific computing in python. *Nature Methods*, (3):261–272, February 2020.
- [26] James Bradbury, Roy Frostig, Peter Hawkins, Matthew James Johnson, Chris Leary, Dougal Maclaurin, George Necula, Adam Paszke, Jake VanderPlas, Skye Wanderman-Milne, et al. Jax: Autograd and xla. *Astrophysics Source Code Library*, pages ascl–2111, 2021.
- [27] Dougal Maclaurin, David Duvenaud, and Ryan P Adams. Autograd: Effortless gradients in numpy. In *ICML 2015 AutoML workshop*, volume 238, 2015.
- [28] Martín Abadi. Tensorflow: learning functions at scale. In *Proceedings of the 21st ACM SIGPLAN International Conference on Functional Programming*, pages 1–1, September 2016.

A Partial derivatives of PQCs

For any $\tilde{U}_t(\boldsymbol{\theta}_t)$ that conforms to

$$\tilde{U}_t(\boldsymbol{\theta}_t) = \prod_{l=1}^L W_l V_l(\boldsymbol{\theta}_{t,l}), \quad (15)$$

we have

$$\begin{aligned} \partial_{l,k} \tilde{U}_t(\boldsymbol{\theta}_t) &= U_{t,L:l+1} W_t \cdot \left[\otimes_{\lambda=0}^{n-1} \prod_{i=0}^{\alpha} R_{\sigma^{(i)}}(\theta_{t,l,\lambda\tau+i}) \cdot \left(-\frac{i}{2} \sigma^{(\alpha)} \delta_{\lambda\tau+\alpha,k} + I \cdot (1 - \delta_{\lambda\tau+\alpha,k}) \right) \right. \\ &\quad \cdot \left. \prod_{i=\alpha+1}^{\tau-1} R_{\sigma^{(i)}}(\theta_{t,l,\lambda\tau+i}) \right] \cdot \tilde{U}_{t,l-1:1} \\ &= -\frac{i}{2} \tilde{U}_{t,L:l} K \tilde{U}_{t,l-1:1}, \end{aligned} \quad (16)$$

where $\alpha = k \bmod \tau$, n is the total number of qubits, $K = (\otimes_{\lambda=0}^{n-1} \prod_{i=\alpha+1}^{\tau-1} R_{\sigma^{(i)}}(\theta_{t,l,\lambda\tau+i}))^\dagger [(I^{0:[k/\tau]} \otimes \sigma^{(\alpha)} \otimes I^{\lfloor k/\tau+1 \rfloor:n}) (\otimes_{\lambda=0}^{n-1} \prod_{i=\alpha+1}^{\tau-1} R_{\sigma^{(i)}}(\theta_{t,l,\lambda\tau+i}))]$, $I^{i:j}$ denotes that the operator I acts on the qubits in the range $[i, j]$. Obviously K is a Hermitian operator.

B Partial derivatives of loss

The loss $\mathcal{L}_t(\boldsymbol{\theta}_t)$ that conforms to $\mathcal{L}_t(\boldsymbol{\theta}_t) = \mathcal{D}_{\text{MMD}}(\tilde{\mathcal{S}}_{t-1}, \mathcal{S}'_{t-1}) = \mathcal{D}_{\text{MMD}}(\tilde{U}_t(\boldsymbol{\theta}_t) \tilde{\mathcal{S}}_t, \mathcal{S}'_{t-1})$ can be regarded as the function of $\tilde{U}_t(\boldsymbol{\theta}_t)$, therefore, we have:

- $\bar{F}(\mathcal{S}'_{t-1}, \mathcal{S}'_{t-1})$ is a constant term, so $\partial_{l,k} \bar{F}(\mathcal{S}'_{t-1}, \mathcal{S}'_{t-1}) = 0$
- For $\bar{F}(\tilde{\mathcal{S}}_{t-1}, \tilde{\mathcal{S}}_{t-1})$, we have

$$\begin{aligned} \bar{F}(\tilde{\mathcal{S}}_{t-1}, \tilde{\mathcal{S}}_{t-1}) &= \mathbb{E}_{|\psi_{t-1}\rangle \in \tilde{\mathcal{S}}_{t-1}, |\phi_{t-1}\rangle \in \tilde{\mathcal{S}}_{t-1}} [|\langle \psi_{t-1} | \phi_{t-1} \rangle|^2] \\ &= \mathbb{E}_{\rho_{\psi_{t-1}} \in \tilde{\mathcal{S}}_{t-1}, \rho_{\phi_{t-1}} \in \tilde{\mathcal{S}}_{t-1}} \text{Tr}(\rho_{\psi_{t-1}} \cdot \rho_{\phi_{t-1}}), \end{aligned} \quad (17)$$

where $\rho_{\psi_{t-1}}$ and $\rho_{\phi_{t-1}}$ are the density matrices of ψ_{t-1} and ϕ_{t-1} , respectively. Then

$$\begin{aligned} \rho_{\psi_{t-1}} &= \text{Tr}_{\text{ancilla}} [\tilde{U}_t(|0\rangle\langle 0| \otimes \rho_{\psi_t})] \\ &= \text{Tr}(\tilde{U}_t^{0:n_a} |0\rangle\langle 0| \tilde{U}_t^{0:n_a \dagger}) \cdot \tilde{U}_t^{n_a+1:n} \rho_{\psi_t} \tilde{U}_t^{n_a+1:n \dagger} \\ &= \tilde{U}_t^{n_a+1:n} \rho_{\psi_t} \tilde{U}_t^{n_a+1:n \dagger}, \end{aligned} \quad (18)$$

where $\text{Tr}_{\text{ancilla}}$ denotes the partial trace over the ancilla qubits to obtain the reduced density operator for the data qubits. $\tilde{U}_t^{0:n_a}$ and $\tilde{U}_t^{n_a+1:n}$ represents the part of \tilde{U}_t applied to the ancilla qubits and data qubits, respectively. Then, we have

$$\begin{aligned} \bar{F}(\tilde{\mathcal{S}}_{t-1}, \tilde{\mathcal{S}}_{t-1}) &= \mathbb{E}_{\rho_{\psi_{t-1}} \in \tilde{\mathcal{S}}_{t-1}, \rho_{\phi_{t-1}} \in \tilde{\mathcal{S}}_{t-1}} \text{Tr}(\rho_{\psi_{t-1}} \cdot \rho_{\phi_{t-1}}) \\ &= \mathbb{E}_{\rho_{\psi_t} \in \tilde{\mathcal{S}}_t, \rho_{\phi_t} \in \tilde{\mathcal{S}}_t} \text{Tr}(\tilde{U}_t^{n_a+1:n} \rho_{\psi_t} \tilde{U}_t^{n_a+1:n \dagger} \cdot \tilde{U}_t^{n_a+1:n} \rho_{\phi_t} \tilde{U}_t^{n_a+1:n \dagger}) \\ &= \mathbb{E}_{\rho_{\psi_t} \in \tilde{\mathcal{S}}_t, \rho_{\phi_t} \in \tilde{\mathcal{S}}_t} \text{Tr}(\rho_{\psi_t} \cdot \rho_{\phi_t}) \\ &= \bar{F}(\tilde{\mathcal{S}}_t, \tilde{\mathcal{S}}_t) \\ &= \bar{F}(\tilde{\mathcal{S}}_T, \tilde{\mathcal{S}}_T). \end{aligned} \quad (19)$$

Therefore, $\bar{F}(\tilde{\mathcal{S}}_{t-1}, \tilde{\mathcal{S}}_{t-1})$ is also a constant term, so $\partial_{l,k} \bar{F}(\tilde{\mathcal{S}}_{t-1}, \tilde{\mathcal{S}}_{t-1}) = 0$.

- For $\bar{F}(\tilde{S}_{t-1}, S'_{t-1})$, we have

$$\begin{aligned}
\partial_{l,k} \bar{F}(\tilde{S}_{t-1}, S'_{t-1}) &= \mathbb{E}_{|\tilde{\psi}_{t-1}\rangle \in \tilde{S}_{t-1}, |\psi_{t-1}\rangle \in S'_{t-1}} \partial_{l,k} [|\langle \tilde{\psi}_{t-1} | \psi_{t-1} \rangle|^2] \\
&= \mathbb{E}_{|\tilde{\psi}_t\rangle \in \tilde{S}_t, |\psi_{t-1}\rangle \in S'_{t-1}} \partial_{l,k} [|\langle \tilde{\psi}_t | \tilde{U}'_t | \psi_{t-1} \rangle|^2] \\
&= \mathbb{E}_{\rho_{\tilde{\psi}_t} \in \tilde{S}_t, \rho_{\psi_{t-1}} \in S'_{t-1}} \partial_{l,k} \text{Tr}[\rho_{\psi_{t-1}} \cdot \tilde{U}'_t \rho_{\tilde{\psi}_t} \tilde{U}'_t{}^\dagger] \\
&= \mathbb{E}_{\rho_{\tilde{\psi}_t} \in \tilde{S}_t, \rho_{\psi_{t-1}} \in S'_{t-1}} \text{Tr}[\rho_{\psi_{t-1}} \cdot \partial_{l,k} \tilde{U}'_t \rho_{\tilde{\psi}_t} \tilde{U}'_t{}^\dagger] \\
&= \frac{1}{|\tilde{S}_t| |S'_{t-1}|} \cdot \left(-\frac{i}{2}\right) \sum_{i,j} \text{Tr}(\rho_{\psi_{t-1,j}} \cdot \tilde{U}'_{t,L:l} [K, \tilde{U}'_{t,l-1:1} \rho_{\tilde{\psi}_{t,i}} \tilde{U}'_{t,l-1:1}{}^\dagger] \tilde{U}'_{t,L:l}{}^\dagger),
\end{aligned} \tag{20}$$

where $|\psi_{t-1,j}\rangle \in \mathcal{S}_{t-1}$, $|\tilde{\psi}_{t,i}\rangle \in \tilde{\mathcal{S}}_t$, \tilde{U}'_t represents the part of \tilde{U}_t applied to the data qubits.

Thus, the partial derivative of the loss function $\mathcal{L}_t(\theta_t)$ with respect to the parameters $\theta_{t,l,k}$ is:

$$\begin{aligned}
\partial_{l,k} \mathcal{L}_t(\theta_t) &= -2 \partial_{l,k} \bar{F}(\tilde{S}_{t-1}, S'_{t-1}) \\
&= \frac{i}{|\mathcal{S}|^2} \sum_{i,j} \text{Tr}(|\psi_{t-1,j}\rangle \langle \psi_{t-1,j}| \cdot \tilde{U}'_{t,L:l} [K, \tilde{U}'_{t,l-1:1} |\tilde{\psi}_{t,i}\rangle \langle \tilde{\psi}_{t,i}| \tilde{U}'_{t,l-1:1}{}^\dagger] \tilde{U}'_{t,L:l}{}^\dagger),
\end{aligned} \tag{21}$$

where $|\mathcal{S}| = |\mathcal{S}_{t-1}| = |\tilde{\mathcal{S}}_{t-1}|$.

C Proof of Theorem 1

Here we give the proof of Theorem.1. For the gradients

$$\partial_{l,k} \mathcal{L}_H = \frac{i}{|\mathcal{S}|^2} \sum_{i,j} \text{Tr}(|\psi_j\rangle \langle \psi_j| \cdot \tilde{U}'_{L:l} [K, \tilde{U}'_{l-1:1} \cdot U_{Hi} |0\rangle \langle 0| U_{Hi}^\dagger \cdot \tilde{U}'_{l-1:1}{}^\dagger] \tilde{U}'_{L:l}{}^\dagger), \tag{22}$$

we provide its mean over the unitary group $\mathcal{U}_H(N)$ which obey Haar measure [23]:

$$\langle \partial_{l,k} \mathcal{L}_H \rangle = \int d\mu(U_H) \frac{i}{|\mathcal{S}|^2} \sum_{i,j} \text{Tr}(|\psi_j\rangle \langle \psi_j| \cdot \tilde{U}'_{L:l} [K, \tilde{U}'_{l-1:1} \cdot U_{Hi} |0\rangle \langle 0| U_{Hi}^\dagger \cdot \tilde{U}'_{l-1:1}{}^\dagger] \tilde{U}'_{L:l}{}^\dagger), \tag{23}$$

We introduce a property of the unitary group matching the Haar distribution [23],

$$\int_{\mathcal{U}_H(N)} u_{ij} \bar{u}_{i'j'} dU_H = \frac{1}{N} \delta_{ii'} \delta(jj'), \tag{24}$$

where u_{ij} and $u_{i'j'}$ are the element of unitary operator U_H . From this we can deduce that

$$\int_{\mathcal{U}_H(N)} d\mu(U_H) U_H V U_H^\dagger = \frac{\text{Tr}(V)}{N} I. \tag{25}$$

Then, we can calculate:

$$\begin{aligned}
\langle \partial_{l,k} \mathcal{L}_H \rangle &= \frac{i}{|\mathcal{S}|^2} \sum_{i,j} \text{Tr}(|\psi_j\rangle \langle \psi_j| \cdot \tilde{U}'_{L:l} [K, \frac{I}{2^{n_{data}}}] \tilde{U}'_{L:l}{}^\dagger) \\
&= 0,
\end{aligned} \tag{26}$$

where n_{data} represent the number of data qubits.

Next, we compute the variance of the gradient Eq.22, which is given as

$$\text{Var}(\partial_{l,k} \mathcal{L}_H) = \langle (\partial_{l,k} \mathcal{L}_H)^2 \rangle - \langle \partial_{l,k} \mathcal{L}_H \rangle^2. \tag{27}$$

Due to $\langle \partial_{l,k} \mathcal{L}_H \rangle = 0$, we can get=

$$\text{Var}(\partial_{l,k} \mathcal{L}_H) = \langle (\partial_{l,k} \mathcal{L}_H)^2 \rangle. \tag{28}$$

Expand as follows:

$$\begin{aligned} \text{Var}(\partial_{l,k}\mathcal{L}_H) = & -\frac{1}{|S|^4} \left(\sum_{b \neq d} \left[\int d\mu(U_{Hb}) \text{Tr}(\rho_{\psi_a} \cdot \tilde{U}'_{L:l}[K, \tilde{U}'_{l-1:1} U_{Hb} |0\rangle \langle 0| U_{Hb}^\dagger \tilde{U}'_{l-1:1}^\dagger] \tilde{U}'_{L:l}^\dagger) \right. \right. \\ & \int d\mu(U_{Hd}) \text{Tr}(\rho_{\psi_c} \cdot \tilde{U}'_{L:l}[K, \tilde{U}'_{l-1:1} U_{Hd} |0\rangle \langle 0| U_{Hd}^\dagger \tilde{U}'_{l-1:1}^\dagger] \tilde{U}'_{L:l}^\dagger) \\ & \left. + \sum_j \left[\int d\mu(U_{Hx}) \text{Tr}(\rho_{\psi_i} \cdot \tilde{U}'_{L:l}[K, \tilde{U}'_{l-1:1} U_{Hx} |0\rangle \langle 0| U_{Hx}^\dagger \tilde{U}'_{l-1:1}^\dagger] \tilde{U}'_{L:l}^\dagger) \right. \right. \\ & \left. \left. \text{Tr}(\rho_{\psi_j} \cdot \tilde{U}'_{L:l}[K, \tilde{U}'_{l-1:1} U_{Hx} |0\rangle \langle 0| U_{Hx}^\dagger \tilde{U}'_{l-1:1}^\dagger] \tilde{U}'_{L:l}^\dagger) \right] \right), \end{aligned} \quad (29)$$

where $\rho_{\psi_k} = |\psi_k\rangle\langle\psi_k|$. After that, we can calculate:

$$\begin{aligned} \text{Var}(\partial_{l,k}\mathcal{L}_H) = & \langle \partial_{l,k}\mathcal{L}_H \rangle^2 - \frac{1}{|S|^4} \sum \left[\int d\mu(U_{Hx}) \text{Tr}(\rho_{\psi_i} \cdot \tilde{U}'_{L:l}[K, \tilde{U}'_{l-1:1} U_{Hx} |0\rangle \langle 0| U_{Hx}^\dagger \tilde{U}'_{l-1:1}^\dagger] \right. \\ & \left. \tilde{U}'_{L:l}^\dagger) \text{Tr}(\rho_{\psi_j} \cdot \tilde{U}'_{L:l}[K, \tilde{U}'_{l-1:1} U_{Hx} |0\rangle \langle 0| U_{Hx}^\dagger \tilde{U}'_{l-1:1}^\dagger] \tilde{U}'_{L:l}^\dagger) \right] \\ = & -\frac{1}{|S|^4} \sum \left[\int d\mu(U_{Hx}) \text{Tr}(\rho_{\psi_i} \cdot \tilde{U}'_{L:l}[K, \tilde{U}'_{l-1:1} U_{Hx} |0\rangle \langle 0| U_{Hx}^\dagger \tilde{U}'_{l-1:1}^\dagger] \tilde{U}'_{L:l}^\dagger) \right. \\ & \left. \text{Tr}(\rho_{\psi_j} \cdot \tilde{U}'_{L:l}[K, \tilde{U}'_{l-1:1} U_{Hx} |0\rangle \langle 0| U_{Hx}^\dagger \tilde{U}'_{l-1:1}^\dagger] \tilde{U}'_{L:l}^\dagger) \right], \end{aligned} \quad (30)$$

We similarly introduce a property of unitary group with respect to the Haar measure [23] to deal with the integral in Eq.30:

$$\begin{aligned} \int_{\mathcal{U}_H(N)} u_{i_1 j_1} u_{i_2 j_2} \bar{u}_{i'_1 j'_1} \bar{u}_{i'_2 j'_2} d\mu(U_H) = & \frac{\delta_{i_1 i'_1} \delta_{i_2 i'_2} \delta_{j_1 j'_1} \delta_{j_2 j'_2} + \delta_{i_1 i'_2} \delta_{i_2 i'_1} \delta_{j_1 j'_2} \delta_{j_2 j'_1}}{N^2 - 1} - \\ & \frac{\delta_{i_1 i'_1} \delta_{i_2 i'_2} \delta_{j_1 j'_2} \delta_{j_2 j'_1} + \delta_{i_1 i'_2} \delta_{i_2 i'_1} \delta_{j_1 j'_1} \delta_{j_2 j'_2}}{N(N^2 - 1)}. \end{aligned} \quad (31)$$

To compute the variance of the gradient, we need to introduce two lemmas.

Lemma 1. Assuming A, B, C, U and V are all N -dimensional unitary matrices, then

$$\text{Tr}(AB[V, CU|0\rangle\langle 0|U^\dagger C^\dagger]B^\dagger) = \sum_{b, b', e, e' < N} D_{ib} U_{b1} U_{1e}^\dagger E_{ei} - F_{jb'} U_{b'1} U_{1e'}^\dagger G_{e'j}, \quad (32)$$

where $D = ABVC, E = C^\dagger B^\dagger, F = ABC, G = C^\dagger VB^\dagger$.

Proof. We have

$$\begin{aligned} & \text{Tr}(AB[V, CU|0\rangle\langle 0|U^\dagger C^\dagger]B^\dagger) \\ = & \text{Tr}(ABVCU|0\rangle\langle 0|U^\dagger C^\dagger B^\dagger - ABCU|0\rangle\langle 0|U^\dagger C^\dagger VB^\dagger) \\ = & \sum (ABVC)_{ib} U_{bc} (|0\rangle\langle 0|)_{cd} U_{de}^\dagger (C^\dagger B^\dagger)_{ei} - \\ & (ABC)_{jb'} U_{b'c'} (|0\rangle\langle 0|)_{c'd'} U_{d'e'}^\dagger (C^\dagger VB^\dagger)_{e'j}. \end{aligned} \quad (33)$$

Letting $D = ABVC, E = C^\dagger B^\dagger, F = ABC, G = C^\dagger VB^\dagger$, we obtain the following result:

$$\begin{aligned} & \text{Tr}(AB[V, CU|0\rangle\langle 0|U^\dagger C^\dagger]B^\dagger) \\ = & \sum D_{ib} U_{bc} |0\rangle\langle 0|_{cd} U_{de}^\dagger E_{ei} - F_{jb'} U_{b'1} |0\rangle\langle 0|_{1e'} U_{1e'}^\dagger G_{e'j} \\ = & \sum_{b, b', e, e' < 2^n \text{ data}} D_{ib} U_{b1} U_{1e}^\dagger E_{ei} - F_{jb'} U_{b'c'} |0\rangle\langle 0|_{c'd'} U_{d'e'}^\dagger G_{e'j}. \end{aligned} \quad (34)$$

□

Lemma 2. Assuming A, B, C, D and U are all N -dimensional unitary matrices, and $U \in \mathcal{U}(N)$ match the Haar distribution. Then, we have

$$|\mathbb{E}_{U \in \mathcal{U}(N)}(\sum A_{ae} U_{e1} U_{1f}^\dagger B_{fa} C_{bg} U_{g1} U_{1h}^\dagger D_{hb})| \in [-\frac{2}{N^2-1}, \frac{2}{N^2-1}]. \quad (35)$$

Proof. We have

$$\mathbb{E}_{U \in \mathcal{U}(N)}(\sum A_{ae} U_{e1} U_{1f}^\dagger B_{fa} C_{bg} U_{g1} U_{1h}^\dagger D_{hb}) = \int d\mu(U) A_{ae} U_{e1} U_{1f}^\dagger B_{fa} C_{bg} U_{g1} U_{1h}^\dagger D_{hb}. \quad (36)$$

By applying Eq.31 and assuming that N is sufficiently large, we obtain the following result:

$$\begin{aligned} \mathbb{E}(\sum A_{ae} U_{e1} U_{1f}^\dagger B_{fa} C_{bg} U_{g1} U_{1h}^\dagger D_{hb}) &\approx \frac{2}{N^2-1} \sum A_{a1} B_{1a} C_{b1} D_{1b} \\ &= \frac{2}{N^2-1} (BA)_{11} (DC)_{11}, \end{aligned} \quad (37)$$

Due to $A, B, C,$ and D are unitary matrices, $|\mathbb{E}(\sum A_{ae} U_{e1} U_{1f}^\dagger B_{fa} C_{bg} U_{g1} U_{1h}^\dagger D_{hb})| \in [-\frac{2}{N^2-1}, \frac{2}{N^2-1}]$. \square

In accordance with Lemma 1, we define $A_k = \rho_{\psi_k} \tilde{U}'_{L:l} K \tilde{U}'_{l-1:1}$, $B = \tilde{U}'_{l-1:1} \tilde{U}'_{L:l} = \tilde{U}'^\dagger$, $C_k = \rho_{\psi_k} \tilde{U}'_{L:l} \tilde{U}'_{l-1:1} = \rho_{\psi_k} \tilde{U}'$, $D = \tilde{U}'_{l-1:1} K \tilde{U}'_{L:l}$ in Eq.30. Then, we obtain the following result:

$$\begin{aligned} \text{Var}(\partial_{l,k} \mathcal{L}_H) &= -\frac{1}{|\mathcal{S}|^4} \sum_{i,j,x} \left\{ \int d\mu(U_{Hx}) [\sum (A_i)_{ab} (U_{Hx})_{b1} (U_{Hx}^\dagger)_{1c} B_{ca} - (C_i)_{de} (U_{Hx})_{e1} \right. \\ &\quad \left. (U_{Hx}^\dagger)_{1f} D_{fd}] \cdot [\sum (A_j)_{a'b'} (U_{Hx})_{b'1} (U_{Hx}^\dagger)_{1c'} B_{c'a'} - (C_j)_{d'e'} (U_{Hx})_{e'1} \right. \\ &\quad \left. (U_{Hx}^\dagger)_{1f'} D_{f'd'}] \right\} \\ &= \frac{1}{|\mathcal{S}|^4} \sum_{i,j,x} \left\{ \int d\mu(U_{Hx}) [-\sum (A_i)_{ab} (U_{Hx})_{b1} (U_{Hx}^\dagger)_{1c} B_{ca} (A_j)_{a'b'} (U_{Hx})_{b'1} \right. \\ &\quad \left. (U_{Hx}^\dagger)_{1c'} B_{c'a'} + \sum (A_i)_{ab} (U_{Hx})_{b1} (U_{Hx}^\dagger)_{1c} B_{ca} (C_j)_{d'e'} (U_{Hx})_{e'1} (U_{Hx}^\dagger)_{1f'} \right. \\ &\quad \left. D_{f'd'} + \sum (C_i)_{de} (U_{Hx})_{e1} (U_{Hx}^\dagger)_{1f} D_{fd} (A_j)_{a'b'} (U_{Hx})_{b'1} (U_{Hx}^\dagger)_{1c'} B_{c'a'} - \right. \\ &\quad \left. \sum (C_i)_{de} (U_{Hx})_{e1} (U_{Hx}^\dagger)_{1f} D_{fd} (C_j)_{d'e'} (U_{Hx})_{e'1} (U_{Hx}^\dagger)_{1f'} D_{f'd'}] \right\} \end{aligned} \quad (38)$$

By applying Lemma2, we obtain the following result:

$$|\text{Var}(\partial_{l,k} \mathcal{L}_H)| \leq \frac{1}{|\mathcal{S}|^4} \cdot \frac{2}{2^{n_{data}} - 1} \cdot 4 = \frac{8}{|\mathcal{S}|^4 (2^{n_{data}} - 1)}. \quad (39)$$

Next, we conduct an analysis of approximate Haar random states. For approximate Haar random states, we present the following properties:

$$\int_{\text{approximate Haar}} U_A \rho U_A^\dagger d(U_A) = \int_{\text{Haar}} U_H \rho U_H^\dagger d(U_H) + \varepsilon, \quad (40)$$

$$\begin{aligned} &\int_{\text{approximate Haar}} (U_A)_{i_1 j_1} (U_A)_{i_2 j_2} (U_A^\dagger)_{i'_1 j'_1} (U_A^\dagger)_{i'_2 j'_2} d(U_A) \\ &= \int_{\text{Haar}} (U_H)_{i_1 j_1} (U_H)_{i_2 j_2} (U_H^\dagger)_{i'_1 j'_1} (U_H^\dagger)_{i'_2 j'_2} d(U_H) + \zeta, \end{aligned} \quad (41)$$

where ε, ζ denote the deviations of approximate Haar random states from exact Haar random states.

Therefore, for

$$\partial_{l,k} \mathcal{L}_A = \frac{i}{|\mathcal{S}|^2} \sum_{i,j} \text{Tr}(|\psi_j\rangle\langle\psi_j| \cdot \tilde{U}'_{L:l} [K, \tilde{U}'_{l-1:1} \cdot U_{Ai} |0\rangle\langle 0| U_{Ai}^\dagger \cdot \tilde{U}'_{l-1:1}] \tilde{U}'_{L:l}), \quad (42)$$

where $U_{Ai} \in \mathcal{U}_A(N)$ obeying approximate Haar measure, it is easy to obtain:

$$\langle \partial_{l,k} \mathcal{L}_A \rangle = \varepsilon, \quad (43)$$

$$\begin{aligned} \text{Var}(\partial_{l,k} \mathcal{L}_A) &= \langle (\partial_{l,k} \mathcal{L}_A)^2 \rangle - \langle \partial_{l,k} \mathcal{L}_A \rangle^2 \\ &= \langle \partial_{l,k} \mathcal{L}_A \rangle^2 - \frac{1}{|\mathcal{S}|^4} \sum \left[\int d\mu(U_{Ax}) \text{Tr}(\rho_{\psi_i} \cdot \tilde{U}'_{L:l}[K, \tilde{U}'_{l-1:1} U_{Ax} | 0] \langle 0 | U_{Ax}^\dagger \tilde{U}'_{l-1:1} \rangle \right. \\ &\quad \left. \tilde{U}'_{L:l} \rangle \text{Tr}(\rho_{\psi_j} \cdot \tilde{U}'_{L:l}[K, \tilde{U}'_{l-1:1} U_{Ax} | 0] \langle 0 | U_{Ax}^\dagger \tilde{U}'_{l-1:1} \rangle \tilde{U}'_{L:l}) \right] - \langle \partial_{l,k} \mathcal{L}_A \rangle^2 \\ &\leq \frac{8}{|\mathcal{S}|^4 (2^{n_{data}} - 1)} + 4\zeta \end{aligned} \quad (44)$$

D Proof of Theorem 2

For convenience, we denote

$$O = I \otimes |\psi\rangle\langle\psi|, \quad (45)$$

$$O_m = G_m^\dagger W_m^\dagger \cdots G_L^\dagger W_L^\dagger O W_L G_L \cdots W_m G_m. \quad (46)$$

and

$$\rho = |\tilde{\psi}\rangle\langle\tilde{\psi}|, \quad (47)$$

$$\rho_m = W_m G_m \cdots W_1 G_1 \rho G_1^\dagger W_1^\dagger \cdots G_m^\dagger W_m^\dagger. \quad (48)$$

Then the function f can be expressed as:

$$\begin{aligned} f &= \text{Tr} [OV(\boldsymbol{\theta})\rho V^\dagger(\boldsymbol{\theta})] \\ &= \text{Tr} [OW_L G_L \cdots W_1 G_1 \rho G_1^\dagger W_1^\dagger \cdots G_L^\dagger W_L^\dagger] \\ &= \text{Tr} [O_{k+1} W_k G_k \rho_{k-1} G_k^\dagger W_k^\dagger] \\ &= \text{Tr} [O_{k+1} W_k \exp[-iH_k \theta_k / 2] \rho_{k-1} \exp[iH_k \theta_k / 2] W_k^\dagger] \\ &= \cos^2 \frac{\theta_k}{2} \text{Tr} [O_{k+1} W_k \rho_{k-1} W_k^\dagger] + \sin^2 \frac{\theta_k}{2} \text{Tr} [O_{k+1} W_k H_k \rho_{k-1} H_k W_k^\dagger] \\ &\quad + \frac{i}{2} \sin \theta_k \left(\text{Tr} [O_{k+1} W_k \rho_{k-1} H_k W_k^\dagger] - \text{Tr} [O_{k+1} W_k H_k \rho_{k-1} W_k^\dagger] \right). \end{aligned} \quad (49)$$

Therefore, the gradient with respect to θ_k is

$$\frac{\partial f}{\partial \theta_k} = \frac{1}{2} \sin \theta_k \text{Tr} [O_{k+1} W_k (H_k \rho_{k-1} H_k - \rho_{k-1}) W_k^\dagger] + \frac{1}{2} \cos \theta_k \text{Tr} [O_{k+1} W_k [\rho_{k-1}, iH_k] W_k^\dagger], \quad (50)$$

where $[A, B] := AB - BA$. Since the expectation of $\sin 2\theta_k$ is zero, it can be shown that

$$\begin{aligned} \mathbb{E}_{\theta_k} \left(\frac{\partial f}{\partial \theta_k} \right)^2 &= \frac{1}{4} \mathbb{E}_{\theta_k} \sin^2 \theta_k \text{Tr} [O_{k+1} W_k (H_k \rho_{k-1} H_k - \rho_{k-1}) W_k^\dagger]^2 \\ &\quad + \frac{1}{4} \mathbb{E}_{\theta_k} \cos^2 \theta_k \text{Tr} [O_{k+1} W_k [\rho_{k-1}, iH_k] W_k^\dagger]^2 \end{aligned} \quad (51)$$

$$\begin{aligned} &= \frac{1}{8} \left(1 - \frac{\sin 2s_k}{2s_k} \right) \text{Tr} [O_{k+1} W_k H_k [\rho_{k-1}, H_k] W_k^\dagger]^2 \\ &\quad + \frac{1}{8} \left(1 + \frac{\sin 2s_k}{2s_k} \right) \text{Tr} [O_{k+1} W_k [\rho_{k-1}, iH_k] W_k^\dagger]^2, \end{aligned} \quad (52)$$

where Eq. (52) is obtained by calculating the integral:

$$\mathbb{E} \cos^2 x = \int_{-a}^a \frac{1}{2a} \cos^2 x dx = \frac{1}{2} \left(1 + \frac{\sin 2a}{2a} \right), \quad (53)$$

$$\mathbb{E} \sin^2 x = \int_{-a}^a \frac{1}{2a} \sin^2 x dx = \frac{1}{2} \left(1 - \frac{\sin 2a}{2a} \right). \quad (54)$$

Next, we focus on the expectation with respect to other parameters. Specifically, the following derivation holds for arbitrary Hermitian X :

$$\mathbb{E}_{\theta_1, \dots, \theta_{k-1}, \theta_{k+1}, \theta_L} \text{Tr} \left[O_{k+1} W_k X W_k^\dagger \right]^2 \quad (55)$$

$$= \mathbb{E}_{\theta_1, \dots, \theta_{k-1}, \theta_{k+1}, \theta_L} \text{Tr} \left[G_{k+1}^\dagger W_{k+1}^\dagger O_{k+2} W_{k+1} G_{k+1} W_k X W_k^\dagger \right]^2 \quad (56)$$

$$= \mathbb{E}_{\theta_1, \dots, \theta_{k-1}, \theta_{k+1}, \theta_L} \text{Tr} \left[\exp[iH_{k+1}\theta_{k+1}/2] W_{k+1}^\dagger O_{k+2} W_{k+1} \exp[-iH_{k+1}\theta_{k+1}/2] W_k X W_k^\dagger \right]^2 \quad (57)$$

$$\begin{aligned} &= \mathbb{E}_{\theta_1, \dots, \theta_{k-1}, \theta_{k+1}, \theta_L} \cos^2 \theta_{k+1} \text{Tr} \left[W_{k+1}^\dagger O_{k+2} W_{k+1} W_k X W_k^\dagger \right]^2 \\ &\quad + \mathbb{E}_{\theta_1, \dots, \theta_{k-1}, \theta_{k+1}, \theta_L} \sin^2 \theta_{k+1} \text{Tr} \left[H_{k+1} W_{k+1}^\dagger O_{k+2} W_{k+1} H_{k+1} W_k X W_k^\dagger \right]^2 \\ &\geq \frac{1}{2} \left(1 + \frac{\sin 2s_{k+1}}{2s_{k+1}} \right) \mathbb{E}_{\theta_1, \dots, \theta_{k-1}, \theta_{k+2}, \theta_L} \text{Tr} \left[W_{k+1}^\dagger O_{k+2} W_{k+1} W_k X W_k^\dagger \right]^2 \end{aligned} \quad (58)$$

$$\geq \prod_{l=k+1}^L \left[\frac{1}{2} \left(1 + \frac{\sin 2s_{k+1}}{2s_{k+1}} \right) \right] \mathbb{E}_{\theta_1, \dots, \theta_{k-1}} \text{Tr} \left[W_{L:k}^\dagger O W_{L:k} X \right]^2, \quad (59)$$

where Eqs. (56) and (57) follow from definitions of O_m and G_l , respectively. Eq. (58) is derived by using the integral in Eq. (53). Eq. (59) is obtained by considering the above derivations for parameters $\theta_{k+2}, \dots, \theta_L$ subsequently. Thus, the expectation of the square of the gradient can be expressed by using Eqs. (52) and (59) as follows:

$$\begin{aligned} \mathbb{E}_{\theta} \left(\frac{\partial f}{\partial \theta_k} \right)^2 &\geq \frac{1}{8} \left(1 - \frac{\sin 2s_k}{2s_k} \right) \prod_{l=k+1}^L \left[\frac{1}{2} \left(1 + \frac{\sin 2s_{k+1}}{2s_{k+1}} \right) \right] \mathbb{E}_{\theta_1, \dots, \theta_{k-1}} \text{Tr} \left[W_{L:k}^\dagger O W_{L:k} H_k [\rho_{k-1}, H_k] \right]^2 \\ &\quad + \frac{1}{8} \left(1 + \frac{\sin 2s_k}{2s_k} \right) \prod_{l=k+1}^L \left[\frac{1}{2} \left(1 + \frac{\sin 2s_{k+1}}{2s_{k+1}} \right) \right] \mathbb{E}_{\theta_1, \dots, \theta_{k-1}} \text{Tr} \left[W_{L:k}^\dagger O W_{L:k} [\rho_{k-1}, iH_k] \right]^2 \end{aligned} \quad (60)$$

$$\begin{aligned} &= \frac{1}{8} \left(1 - \frac{\sin 2s_k}{2s_k} \right) \prod_{l=k+1}^L \left[\frac{1}{2} \left(1 + \frac{\sin 2s_l}{2s_l} \right) \right] \mathbb{E}_{\theta_1, \dots, \theta_{k-1}} \text{Tr} \left[\rho_{k-1} [H_k, W_{L:k}^\dagger O W_{L:k} H_k] \right]^2 \\ &\quad + \frac{1}{8} \left(1 + \frac{\sin 2s_k}{2s_k} \right) \prod_{l=k+1}^L \left[\frac{1}{2} \left(1 + \frac{\sin 2s_l}{2s_l} \right) \right] \mathbb{E}_{\theta_1, \dots, \theta_{k-1}} \text{Tr} \left[\rho_{k-1} [iH_k, W_{L:k}^\dagger O W_{L:k}] \right]^2 \end{aligned} \quad (61)$$

$$\begin{aligned} &\geq \frac{1}{8} \left(1 - \frac{\sin 2s_k}{2s_k} \right) \prod_{l=1, l \neq k}^L \left[\frac{1}{2} \left(1 + \frac{\sin 2s_l}{2s_l} \right) \right] \text{Tr} \left[W_{k-1:1} \rho W_{k-1:1}^\dagger [H_k, W_{L:k}^\dagger O W_{L:k} H_k] \right]^2 \\ &\quad + \frac{1}{4} \prod_{l=1}^L \left[\frac{1}{2} \left(1 + \frac{\sin 2s_l}{2s_l} \right) \right] \text{Tr} \left[W_{k-1:1} \rho W_{k-1:1}^\dagger [iH_k, W_{L:k}^\dagger O W_{L:k}] \right]^2. \end{aligned} \quad (62)$$

Eq. (61) is derived by noticing $\text{Tr}[A[B, C]] = \text{Tr}[ABC - ACB] = \text{Tr}[BCA - BAC] = \text{Tr}[B[C, A]]$. Eq. (62) is derived similar to Eqs. (55-59). By replacing the notations of O and

ρ , we obtain

$$\begin{aligned} \mathbb{E}_{\theta} \left(\frac{\partial f}{\partial \theta_k} \right)^2 &\geq \left(\frac{\partial f}{\partial \theta_k}(\mathbf{0}) \right)^2 \prod_{l=1}^L \left(\frac{1}{2} + \frac{\sin 2s_l}{4s_l} \right) \\ &+ H_{kk}(\mathbf{0})^2 \left(\frac{1}{2} - \frac{\sin 2s_k}{4s_k} \right) \prod_{l=1, l \neq k}^L \left(\frac{1}{2} + \frac{\sin 2s_l}{4s_l} \right) \end{aligned} \quad (63)$$

and prove Theorem 2.

E Algorithm

In this section, we provide the algorithm details of QuDDPM for better understanding.

Algorithm 1: Diffusion

Data: The state ensemble sampled from the target distribution.

Result: The state ensemble generated at each timestep of the diffusion process.

```

1 real_data[0] ← initial_state
2 diff_hs ← linspace(h_start, h_end, T)
3 for t = 1 ... T do
4   | θ ∼ U(− $\frac{\pi}{8}$ ,  $\frac{\pi}{8}$ )
5   | real_data[t] ← QSC(real_data[t-1], θ·diff_hs[t])
6 end

```

Algorithm 2: Denoising

Data: The initial input of the denoising process and the state ensemble generated at each timestep of the diffusion process.

Result: The trained model

```

1 generate_data[T] ← the initial input of the denoising process
2 for t = T-1 ... 0 do
3   | θ ∼ N(0, 1)
4   | for epoch = 0 ... iterations-1 do
5     | generate_data[t] ← PQC(generate_data[t+1], θ)
6     | Take gradient descent step on
7     |   ∇θ DMMD(generate_data[t], real_data[t])
8   | end
9 end

```

F Experiment detail

F.1 Experiments computer resources

All experiments were carried on an NVIDIA GeForce RTX 3090 GPU, which comes equipped with 24GB of memory.

F.2 Licenses for existing assets

The existing assets we use in the experiments are as follows:

- pennylane [24] version 0.38.0 [Apache-2.0 License]
- scipy [25] version 1.13.1 [3-Clause BSD License]
- jax [26] version 0.4.30 [Apache-2.0 License]
- autograd [27] version 1.7.0 [MIT License]
- tensorflow [28] version 2.17.0 [Apache-2.0 License]

G Results Presentation of Diffusion Process

From Fig. 6, we can observe that as the timesteps progress, the data generated by the original QuDDPM's diffusion process rapidly approaches the Haar distribution, and the final diffusion result conforms to the Haar distribution. In contrast, the improved QuDDPM exhibits a slower diffusion rate, and its final diffusion result maintains a certain distance from the Haar distribution, which aligns with our design specifications.

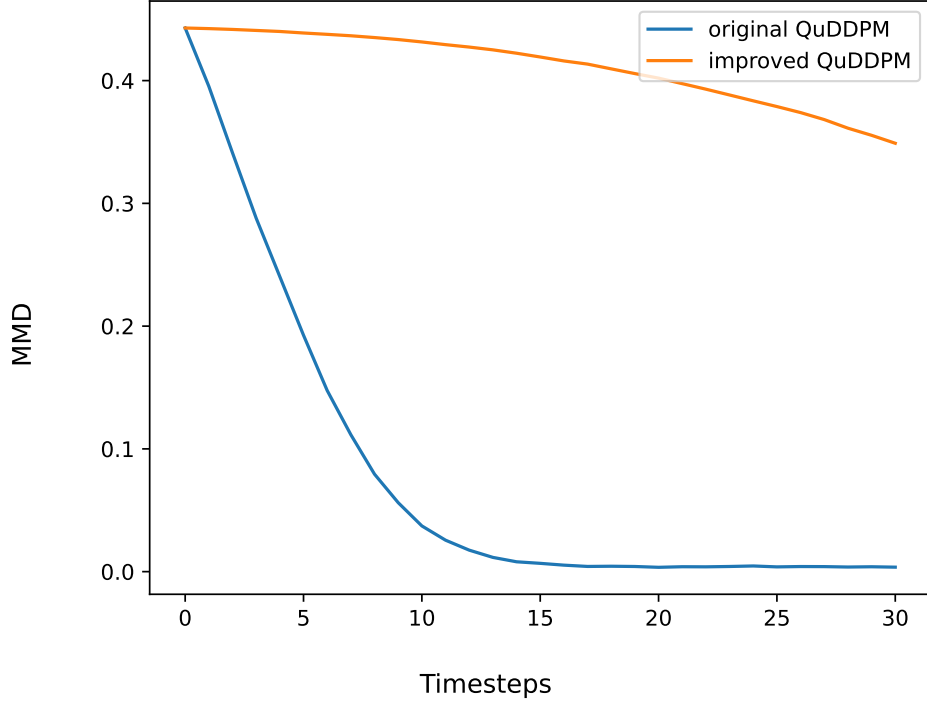


Figure 6: For a quantum system with 4 qubits, this figure shows the Maximum Mean Discrepancy (MMD) between the dataset generated at each timestep of the diffusion process and the true Haar distribution. The orange curve represents the improved QuDDPM, and the blue curve represents the original QuDDPM.

H Supplementary experiments to demonstrate barren plateaus

As shown in Fig. 7 and 8, during the initial training of the denoising process, the training gradient of the original QuDDPM exponentially decreases with the increasing number of qubits, triggering the barren plateau phenomenon and rendering the model untrainable.

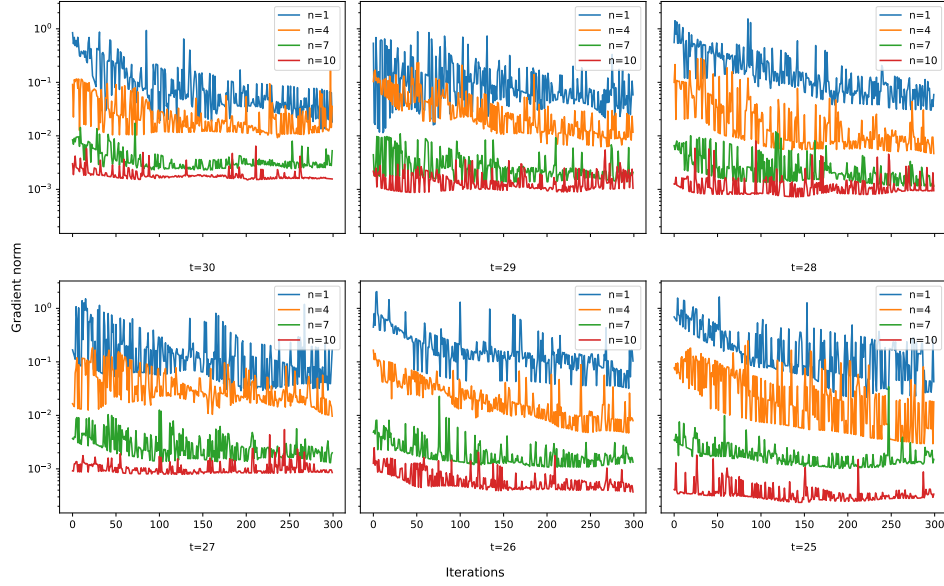


Figure 7: The evolution of the gradient during the first six training cycles of the backward denoising process for different numbers of qubits

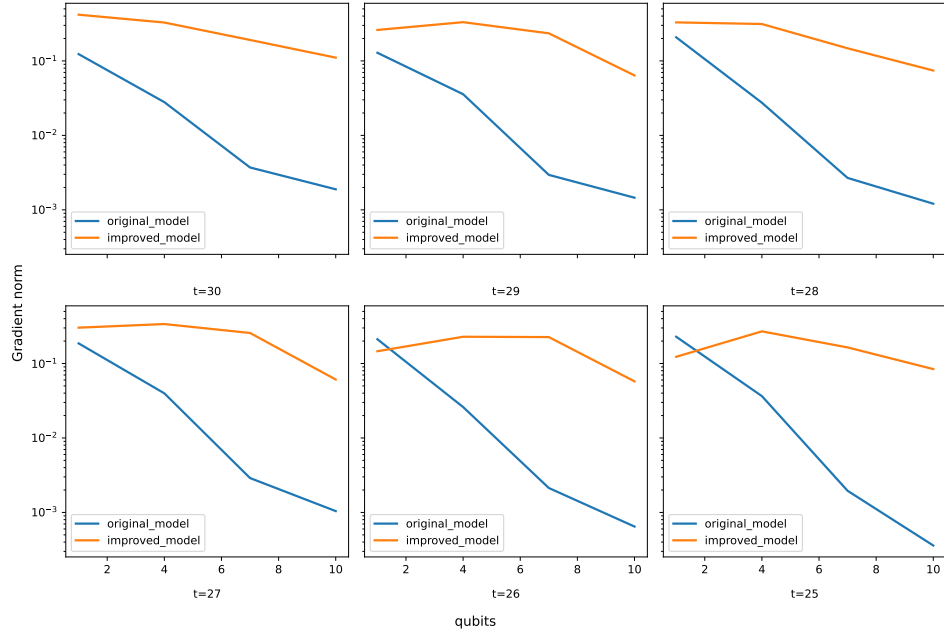


Figure 8: The change in the average gradient of the loss function during the first six training cycles of the reverse denoising process as the number of qubits increases

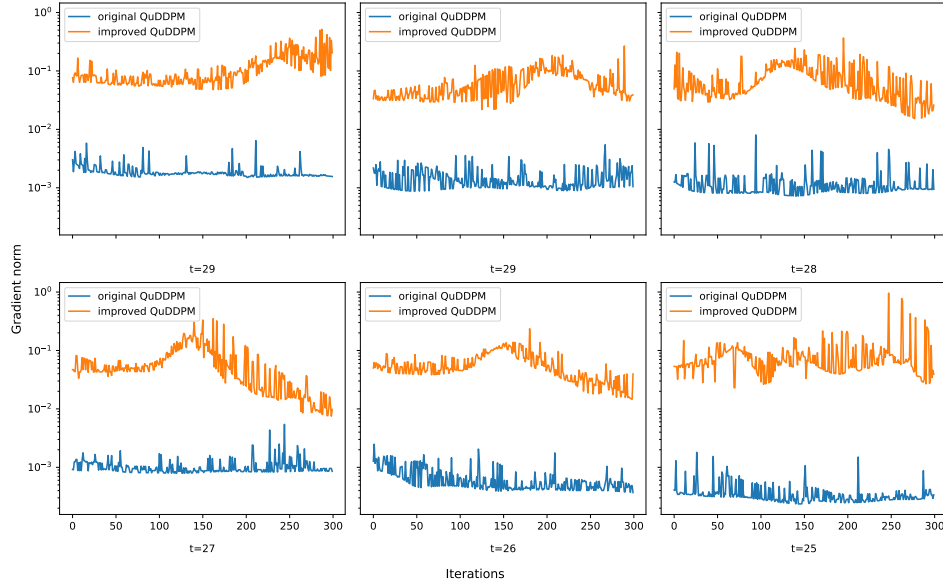


Figure 9: A comparison of the gradients evolution during training between the improved QuDDPM and the original QuDDPM for 10 qubits.

I Supplementary experiments comparing the improved QuDDPM with the original QuDDPM

As shown in Fig. 9, the training gradient of the improved QuDDPM during the early stages of the denoising process is different from that of the original QuDDPM. Its training gradient remains at a normal level, effectively mitigating the barren plateau phenomenon.